PHASE DIAGRAM AND FAST ION TRANSPORT IN NaF-NaBr SYSTEM

by

M Sudha Siva Rani

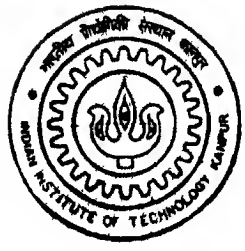

MATERIALS SCIENCE PROGRAMME

INDIAN INSTITUTE OF TECHNOLOGY, KANPUR

February, 2001

PHASE DIAGRAM AND FAST ION TRANSPORT IN NaF-NaBr SYSTEM

A Thesis submitted
in partial fulfillment of the requirement
for the Degree of
MASTER OF TECHNOLOGY

By
M Sudha Siva Rani

To the
MATERIALS SCIENCE PROGRAMME
INDIAN INSTITUTE OF TECHNOLOGY, KANPUR
February 2001

22 2 201

CERTIFICATE

It is certified that the work presented in the thesis entitled, **'Phase-diagram and Fast ion transport in NaF-NaBr system"** by M Sudha Siva Rani has been carried out under my supervision and that this work has not been submitted elsewhere for a degree

February, 2001

(Dr K Shahi)
Supervisor
Materials Science Program
I I T Kanpur

ABSTRACT

NaF – NaBr binary phase diagram has been investigated by means of XRD and thermal analysis (TA) Besides the ac/dc electrical conductivity (σ) is examined as a function of temperature (200 - 650°C) and frequency (5 Hz – 13MHz) for sixteen different compositions in the NaF–NaBr system The variation of transport properties with composition (x) is correlated with the phase diagram It is observed that the addition of just ~*1m o* NaBr in NaF leads to an order of magnitude increase in the conductivity while *2* or *3m o* NaBr in NaF produces no further change in the conductivity However *5m/o* NaBr in NaF leads to further sharp rise in the conductivity The lattice loosening (LL) model for the solid-solution region and the percolation models for the two-phase region are used to explain the seemingly peculiar results The significant enhancement in the conductivity of NaF + *1m/o* NaBr is explained using the LL model on account of a large mismatch (47 %) in the ionic radii of the host F and the dopant Br ions The existence of the percolation threshold as predicted by the percolation models is very well demonstrated by our results on NaF – NaBr system

ACKNOWLEDGEMENT

I express my sincere thanks to Dr K Shahi my thesis supervisor for his constant encouragement and inspiring guidance throughout the course of my work It was a great pleasure to work with him

I am grateful to Mr Uma Shankar Mr B Sharma Mr T B Pandey and Mr Sampati Singh for their technical contributions

Heartfelt thanks are due to my friends S Srikanth U D Saibaba N Sundar Raju, N Neelima Sreya Dutta Animesh Kundu G Srilaxmi Anamika Sethia, Pratheeba ,Praveen Kumar and Arpana Jindal for constantly helping me and making my stay at I I T Kanpur a memorable one

My profound regards are due to my labmates Anshuman Dalvi J P Tiwari, Ashotosh Tiwari Feroz Khan, Manish Raj and Anoop Pant for their co-operation, suggestions and encouragement I take this opportunity to express my sincere thanks to my classmates Abhishek Srivastava and Neeraj Singh

Last but not the least, I am deeply indebted to my parents sister and Krishna Prasad for their ceaseless inspiration and constant encouragement

CONTENTS

LIST OF FIGURES

LIST OF TABLES

Chapter 1

Introduction

1 1 General review

Solid electrolytes are solid state materials which possess an electric conductivity partly or wholly due to ionic displacements Solid electrolytes have been known since 1830 s when charge transport was observed in solids like Ag_2S and PbF_2 by Faraday Tubandt et al [1] made systematic studies on conductivities of these materials They established the Faraday s laws of electrolysis and demonstrated that α-AgI was a pure cationic conductor and $PbCl_2$ was an anionic conductor

In a perfect ionic crystal it is not possible to have large-scale displacements of atoms But a real crystal always has some point defects (vacancies and interstitials) in thermodynamic equilibrium to reduce its free energy These defects are responsible for charge and mass transport in ionic solids In ionic crystals of type MX Schottky defects are characterized by the presence of equal number of anion and cation vacancies Schottky defects are more dominant in alkali halides Presence of equal number of vacancies and interstitials, dominant in silver halides, are Frenkel defects Vacancy mechanism is responsible for charge transport in solids where Schottky defects are dominant Interstitial and interstitialcy mechanisms are responsible for charge transport in solids exhibiting Frenkel defects

1 1(a) classification of solid ionic conductors

The solid ionic conductors can be classified on the basis of nature of charge carriers as

i Cationic conductors

ii Anionic conductors

Based on the structure the solid ionic conductors can be grouped into four classes

i Crystalline ionic conductors

ii Amorphous solid electrolytes

iii Polymeric solid electrolytes

iv Composite solid electrolytes

Based on the magnitude of conductivity of various solid ionic conductors they can be grouped into three categories

i Poor ionic conductors $(\sigma \leq 10^{-6} \Omega^{-1} cm^{-1})$

example Alkali halides

ii Moderate ionic conductors $(10^{-6} \leq \sigma \leq 10^{-3} \Omega^{-1} cm^{-1})$

example AgBr β-AgI CaF_2 PbF_2, CaO ZrO_2

iii Superionic conductors $(\sigma \geq 10^{-3} \Omega^{-1} cm^{-1})$

example α AgI $RbAg_4I_5$ β-Alumina etc

The conductivity of ionic solids is a product of two exponential functions of temperature concentration of defects and mobility of these defects

(section 1 3) The mobility of defects in all normal salts lies in the range 10^{-1} to $10^{6} cm^{2} V^{-1} S^{-1}$ Thus concentration of defects is largely responsible for determining the magnitude of conductivity of the solid ionic conductor at a given temperature Thus the above classification can also be arrived at on the basis of concentration of defects[2]

On the basis of concentration of defects the ionic conductors can be classified as under

i Poor ionic conductors or dilute point defect type $(n \leq 10^{17}/cm^{3})$

ii Moderate ionic conductors or concentrated point defect type $(n \sim 10^{20}/cm^{3})$

iii Superionic conductors $(n \sim 10^{22}\ cm^{3})$

1 2Past work

Lot of work has been done to develop solid state materials, that exhibit high ionic conductivities due to their potential applications in solid state batteries fuel cells etc Several techniques have been employed to enhance the conductivity of pure solids

1 2(a) Stabilization of "average" or disordered structure

High ionic conductivity observed in α-AgI[3 4 5] has been attributed to it's unique structure It has BCC structure in which anions (I ions) occupy corner as well as body center positions There are now 42 interstitial sites

available for 2 Ag^{2+} ions The probability of occupancy of these sites is much less than unity This situation is described as average structure α-Li_2SO_4 is another superionic conductor which has the average structure with β - α transition temperature at ~575°C Several efforts have been put into stabilizing its average structure ' at/near room temperature[6 7] Table 1 1 lists some superionic solids which owe their high ionic conductivity to average structure

Table1 1 some selected superionic conductors with "average" or "molten" sub-lattice structure

compound	mobile ion	ionic(β) superionic(α) transition temperature (^{0}C)	σ ($\Omega^1 cm^1$) (at T^{0}C)
α-Ag_2S	Ag^+	175	4 1 (200)
α-Ag_2Se	Ag^+	133	3 1(200)
α-AgI	Ag^+	147	1 3(150)
α-Ag_3SI	Ag^+	235	2(240)
α-Na_2WO_4	Na^+	589	1 5 x 10^2(800)
α-Li_2SO_4	Li^+	575	1 03(600)

1 2(b) Dispersion of fine insulating particles

Dispersion of fine insulating alumina particles was used to increase the conductivity of LiI[8] Shahi et al [9] showed that increase in conductivity is not just limited to dispeision of insulating particles as alumina fly ash etc but even dispersion of AgBr in β AgI shows orders of magnitude increase in conductivity Such solid electrolytes are known as composite solid electiolytes

Examples of composite solid electiolytes

LiI – Al_2O_3 [8]

AgI Al_2O_3[9]

Na_2SO_4[6]

1 2(c) Doping

Aliovalent doping is doping with ions whose valancy is different from that of the host ion Koch and Wagner[10] Kelting and Witt[11] Teltow[12] have reported increase in conductivity of solid ionic conductors due to aliovalent dopants An aliovalent dopant increases the concentration of certain kind of defects as demanded by the charge neutrality condition

Homovalent doping is doping with ions that have the same valancy as that of the host ions Table 1 2 lists some mixed crystals and their conductivities at appropriate temperatures An inspection of this Table would reveal that the conductivity enhancement ranges from a factor of 10 to 1000

Table 1 2 The electrical conductivity (σ_s) of some mixed crystals and the conductivity enhancement (σ_s/σ_0) relative to that of pure component(σ_0) at a temperature T^{0}C

system	temperature (T^{0}C)	conductivity at T^{0}C ($\sigma_s\ \Omega^{-1}cm^{-1}$)	σ_s σ_0 at T^{0}C
AgI+4m/o AgBr[9]	25	4.3×10^{-6}	16
AgBr+30m/o AgI[9]	25	6.5×10^{-6}	77
Kbr+50m/o KI[9]	500	2.9×10^{-4}	63
KBr+70m/o KI[13]	596	4.5×10^{-5}	9
NaCl+47m/o NaBr[14]	393	8×10^{-5}	10

1 3Theoretical aspects

1 3(a) Conductivity in pure ionic solids

The motion of charged defects in an electric field gives rise to an ionic conductivity which usually dominates the electrical behavior of an ionic crystal because electronic conductivity is absent The general form of Ohm s law says that the current density is proportional to the electric field

$$J = qV_{drift}x = q\mu xE = \sigma E \quad - \quad (1\ 1)$$

where J is the current density

q is the charge on the defect

x is the concentration of defects

μ is the mobility of defects

V_{drift} is the drift velocity acquired by the charge carrier in the presence of an external electric field E

and σ is the conductivity

So expression for conductivity is given by

$$\sigma = q\mu x \qquad (1\ 2)$$

For a MX type of ionic solid, the total conductivity should include contribution from both positively and negatively charged defects So the most general expression for conductivity of an ionic solid is

$$\sigma = \sigma_+ + \sigma = q\mu_+ x_+ + q\mu x \quad ---(1\ 3)$$

where the symbols have their usual meaning

Defect concentrations in pure crystals

Schottky defects

In an ionic crystal of type MX the production of Schottky defects can be envisaged as the removal of a cation and an anion from the interior to the surface of the crystal, leaving a cation and an anion vacancy respectively and can be represented by the reaction equation

$$crystal \leftrightarrow V'_M + V \quad ---(1\ 4)$$

°kroger (1970) notation has been used for representing the defects

This process requires energy but also allows an increase in configurational entropy so that the usual procedure for minimizing the free energy gives

$$x'_{os} = x_{+}x = exp(\frac{-G}{kT}) \quad ---(1\ 5)$$

where x_{+} and x are the mole fractions of cation and anion vacancies respectively The Gibbs free energy G_s is usually written as

$$G_s = H_s - TS_s \quad --(1\ 6)$$

where H_s is the enthalpy of formation of a pair of separated Schottky defects and S_s is the corresponding entropy change (in addition to the configurational entropy) and arises from changes in vibrational frequencies in the vicinity of vacancies[15]

The Schottky product then becomes

$$x^2_{os} = x_{+}x = \exp(\frac{S}{k})\exp(\frac{-H}{kT}) \quad --(1\ 7)$$

Thus the entropy S_s and enthalpy H_s of formation appear as parameters that determine respectively the pre-exponential factor and the temperature dependence

For a pure crystal with only Schottky defects the condition of electric neutrality requires $x_{+} = x$ So

$$x_{os} = x_{+} = x = \exp(\frac{S}{2k})\exp(\frac{-H}{2kT}) \quad --(1\ 8)$$

Frenkel defects

Frenkel defects are formed by removal of a cation /anion from a lattice site and inserting it into an interstitial position

$$Crystal \leftrightarrow V_M + M_i \quad ---(1\ 9)$$

The corresponding Frenkel product is

$$K'_{oF} = x_+ x_i = Z_i \exp(\frac{S_F}{k}) \exp(\frac{-H_F}{kT}) \quad - (1\ 10)$$

where Z_i is the ratio of the interstitial to lattice sites per unit cell

For a particular crystal the type of defect with the lowest formation enthalpy is usually predominant, but when several types of defects are present together, the concentrations are interrelated by the simultaneous operation of several of the mass action equations such as equations *(1 7)* and *(1 10)*

Mobility of defects

The Nernst-Einstein relation expresses the relationship between mobility and diffusion as

$$\mu = \left(\frac{q}{kT}\right) d \quad - (1\ 11)$$

where d is the diffusion coefficient and other symbols have their usual meaning

This relation has been deduced on very general grounds of statistical mechanics[16] and must always be valid in it s microscopic form

Simplified form of equation *(1 11)*[17] yields the following expression

$$\mu = 4\left(\frac{q}{kT}\right)\nu\, a \quad \exp\left(\frac{S}{k}\right)\exp\left(\frac{-H_{,}}{kT}\right) \quad \text{- -(1 12)}$$

where a_o is half of the crystallographic unit cell edge

ν is the attempt frequency

S_m and H_m are the entropy and enthalpy of migration respectively

Thus from equations *(1 2) (1 8) and (1 12)* we see that the conductivity of an ionic crystal is the product of two exponential functions of temperature

1 3(b) Ionic conduction in mixed crystals

Lattice-loosening model (single phase mixed crystals)

In case of aliovalent doping the concentration of certain kind of defects increases in order to satisfy the charge neutrality condition thus leading to an enhancement in the conductivity with respect to the pure solids[18] But in case of homovalent doping the enhancement in conductivity can not be explained using above argument A semi quantitative theory the lattice loosening model was proposed by Shahi and Wagner[19] in order to explain the conductivity enhancement in case of homovalent doping According to the lattice loosening model the substitution of an ion different in size than the host ion introduces strain in the lattice and eventually results in lowering of the formation and migration enthalpies of the point defects thus increasing their concentration and mobility leading to enhanced ionic conductivity

Concentration of defects

Table 1 3 lists the formation enthalpy (H_s) and melting point (T_m) data for some compounds It was first pointed out by Barr et al [20] that H_s and T_m are linearly related as

$$H_s = \alpha T_m \quad \text{---(1 13)}$$

Where α is the proportionality constant and has a value of $\approx 2\ 14\times10^{-3}$ eV/K Equation *(1 13)* in case of mixed crystals can be written as

$$H = \alpha T_M \quad \text{-(1 14)}$$

$$H - H = \alpha(T_M - T_M) \text{- -(1 15)}$$

$$\text{or } \Delta H = \alpha \Delta T_M \text{-} \quad \text{(1 16)}$$

where the unprimed quantities correspond to the pure salt and the primed quantities correspond to the mixed crystal

The expression for the concentration of Schottky defects (Eqn *(1 8)*) in case of mixed crystals can be written as

$$x' = A' \exp\left(\frac{-H}{2kT}\right) \quad \text{--(1 17)}$$

The ratio of the concentration of Schottky defects in the mixed crystal to that in the pure crystal is given by

$$\frac{x}{x} = \frac{A}{A} \exp\left[\frac{-(H' - H)}{2kT}\right] \quad \text{---(1 18)}$$

substituting Eqn *(1 16)* in Eqn *(1 18)*, we have

$$\frac{x'}{x} = \frac{A}{A} \exp\left[\frac{-\alpha \Delta T_m}{2kT}\right] \quad \text{- -(1 19)}$$

The pre-exponential factor in Eqn *(1 19)* depends on the difference in the entropy of formation of defects in pure and mixed crystals Since the

formation entropys in pure and mixed crystals will not be very different from each other the pre-exponential factor in Eqn *(1 19)* can be taken to be of the order of unity[19] Thus the ratio of the concentrations of vacancies in mixed crystal to that of the pure salt can be expressed as

$$\frac{x}{x} = \exp\left[\frac{-\alpha\Delta T_m}{2kT}\right] \quad \text{- (1 20)}$$

Table 1 3 Enthalpy of formation and migration for some ionic solids

compound	Melting point (^{0}C)	formation enthalpy (eV)	enthalpy of migration cation vacancies (eV)	enthalpy of migration anion vacancies (eV)
NaF	992	2 42 – 3 0	0 52 – 0 95	1 46
NaCl	800	2 18 – 2 38	0 66 – 0 76	0 9 – 1 1
NaBr	755	1 72	0 8	1 18
KF	846	2 64 – 2 72	0 84 – 1 02	1 35 – 1 65
KCl	768	2 26 – 2 31	0 71	0 67 – 1 04
KBr	728	2 3 – 2 53	0 62 – 0 67	0 87 – 0 95
KI	680	0 6 – 2 2	0 6 – 1 21	0 5 – 1 5
CsCl	636	1 86	0 6	0 34
CsBr	636	2 0	0 58	0 27
CsI	621	1 9	0 58	0 3

Eqn *(1 20)* predicts an increase in the defect concentration in case of mixed crystals as their melting point is generally lower than that of the pure salt

Mobility of defects

Table 1 2 also lists the enthalpy of migration (H_m) for some ionic compounds The enthalpy of migration depends upon the melting temperature of the salt according to the following equation[17]

$$H_m = \beta T_m \quad \gamma \quad \text{- (1 21)}$$

where β and γ are constants equal to $0\,84\times10^{3}$ eV/K and 0 2 eV respectively

Thus the difference in enthalpy of migration of mixed crystal and pure salt can be expressed as

$$\Delta H_m = \beta\, \Delta T_m \qquad \text{-(1 22)}$$

assuming that the entropy of formation of defects in mixed crystal equals the entropy of formation of defects in pure salt the ratio of mobility of vacancies in mixed crystal to that of the pure salt can be expressed as

$$\frac{\mu}{\mu} \approx \exp\left(\frac{-(H_m - H_m)}{kT}\right) \quad \text{- (1 23)}$$

using Eqn *(1 22)*, we have

Eqn *(1 24)* predicts an enhancement in the mobility of defects in mixed crystals as the melting point of mixed crystals is generally lower than that of the pure salts

Thus from equations *(1 20)* and *(1 24)* the ratio of conductivities of mixed crystal and the pure salt can be expressed as

$$\frac{\sigma}{\sigma} = \frac{x}{x}\frac{\mu}{\mu} = \exp\left[\frac{-(\frac{\alpha}{2}+\beta)\Delta T_n}{kT}\right] \quad - \ (1\ 25)$$

substituting the values of constants α β and k we have

$$\frac{\sigma}{\sigma} = \exp\left(\frac{-22\ 17\Delta T_n}{T}\right) \quad -- \ (1\ 26)$$

The above expression can thus be used to predict the enhancement in conductivity of ionic salts due to homovalent doping

1 3(c) Ionic conduction in multiphase systems

Percolation model

Maxwell's theory[21] predicts that the dispersion of insulating particles in an ionic conductor should decrease the conductivity of the ionic conductor But large enhancement in conductivity has been observed by the dispersion of insulating particles like fly-ash, alumina in a number of ionic conductors like AgI AgBr[9] etc Several theories have been proposed to explain the observed conductivity enhancement in various systems

Jow and Wagner[22] suggested that the enhancement in conductivity is due to the enhancement in defect concentration in the charged double layer that exists at the interface of two different phases The existence of space charge regions near the lattice discontinuities (free surfaces dislocations and grain boundaries etc) in an ionic crystal was first proposed by Frenkel[23] The origin of space charge is ascribed to the difference in the free energy of formation of the individual vacancies in the case of Schottky defects and of the vacancies and interstitials in the case of Frenkel disorder near the lattice discontinuities In the bulk of a crystal an individual component of a defect pair cannot be created without simultaneously creating the other charge compensating defect type However it could be formed separately at the heterogeneity such as free surfaces and lattice discontinuities Thus if the free energy of formation of an interstitial is less than that of a vacancy a greater number of positive interstitials than negative vacancies will be injected giving rise to a net negative surface charge This surface charge is compensated by a near surface region enriched with vacancies The equilibrium distribution of the point defects in the space charge region is such as to screen the deep interior of the crystal from the surface charge

With the basic assumption that the enhancement in conductivity of composite solid electrolytes is due to the formation of a space charge layer, the percolation model has been introduced[24] The percolation model considers the problem of conductivity enhancement in composite solid electrolytes from the macroscopic point of view

lattice has randomly occupied squares with probability p and in three dimensions unit cubes occupy simple cubic lattice with probability p Physically the occupied space for both the cases represent the dispersed second phase particles The bonds connecting the two neighboring sites are regarded as electrical resistors Three types of bonds could be distinguished, highly conducting bonds with interface conductance σ_1 and two normally conducting bonds with interface conductance σ_B and σ_C For the square lattice the bonds have conductance σ_1 if they belong to one occupied square σ_C if they belong to two occupied squares and σ_B if both the squares are empty In the case of cubic lattice the bonds have conductivity σ_1 if they belong to either one, two or three occupied cubes and σ_C if they belong to four occupied cubes, and σ_B if all four cubes are empty The fractions f_1 f_B and f_C of highly conducting and two normally conducting bonds with different conductivitys depend on the concentration p of the dispersoid For a square lattice the corresponding fractions can be written as

$$f_C = p^2 \quad \text{---(1 27)}$$

$$f_B = (1-p)^2 \quad \text{---(1 28)}$$

$$f_1 = 1-f_B f_C$$

$$= 2p(1-p) \quad \text{- -(1 29)}$$

In case of a cubic lattice four neighboring cubes should be occupied to generate a bond with conductivity σ_C and four neighboring cubes should be empty to generate a bond with conductivity σ_B Thus the fractions of the corresponding bonds become

$$f_C = p^4 \quad \text{---(1 30)}$$

$$f_B = (1-p)^4 \quad \text{- (1 31)}$$

$$f_C = p^4 \quad \text{---(1 30)}$$

$$f_B = (1-p)^4 \quad \text{-(1 31)}$$

$$f_1 = 1-f_B f_C$$

$$= 2p(1\ p)\{2-p(1-p)\} \quad \text{- (1 32)}$$

In order to determine quantitatively the total conductivity of the composite material, the three types of bonds are mapped onto the problem of random walk on a lattice The three types of bonds are represented by three different jump rates $(\tau_A)^{-1}$ $(\tau_B)^{-1}$ and $(\tau_C)^{-1}$ which are proportional to the corresponding conductances The walker jumps between the sites, which are the end points of the bonds The following rules of the random walk are used

(i) The probability Π_δ that a walker takes a jump from a given site to one of its nearest neighbors in the direction δ is proportional to the hopping rate $(\tau_\delta)^{-1}$ in that direction

$$\text{i e} \qquad \Pi_\delta = \frac{\tau_\delta^{-1}}{\sum_{\delta=1}^{Z} \tau_\delta^{-1}} \quad \text{-- (1 33)}$$

$$\text{since} \qquad \sum_{\delta\ 1}^{Z} \tau_\delta^{-1} = 1$$

(ii) The total elapsed time t after N_A steps along highly conducting bonds and N_B and N_C steps along the two normally conducting bonds is

$$t = N_A\tau_A + N_B\tau_B + N_C\tau_C \quad \text{-- (1 34)}$$

(iii) For large times t, the mean square displacement of the walker $\langle r^2(t)\rangle$ is proportional to D(p)t D(p) is the diffusion constant which is proportional to the conductivity in accordance with Nernst-Einstein

relation The problem is solved by Monte Carlo simulations From the asymptotic behavior of $\langle I \ (t)\rangle$ one can determine the total conductivity of the system

The solution of the problem gives two critical concentrations of the insulating bonds namely p and $p \ p$ is related to the onset of the enhanced conductivity and defines the lowest concentration of the insulating bonds where an infinite network of highly conducting bonds is formed (interface percolation) p corresponds to the percolation threshold when all the interface bonds get disrupted For simple square and cubic lattice types p and p are connected by the relation $p = 1 - p$

1 4 Present investigation

With the motivation for developing cost effective solid electrolytes the NaF – NaBr mixed crystal system has been chosen Na^+ ions are light and also strongly electropositive and thus can be used for high-energy batteries NaF and NaBr have been chosen because of large mismatch in the ionic radii of fluoride and bromide ions thus expecting a large conductivity enhancement in the solid solution region as suggested by the lattice-loosening model Also a large enhancement in conductivity in the two-phase region is expected due to large difference in the formation energies of the defects in NaF and NaBr[17]

Chapter 2

Characterization Techniques and Experimental Details

2 1 Structural analysis

Different phases of the same material may exhibit different electrical behavior For example β - phase of AgI is a normal ionic conductor whereas α - phase of AgI is a superionic conductor[3 17]

In order to identify the various phases present in the samples to be analyzed for their electrical behavior x-ray diffraction patterns have been taken and analyzed

The X-ray diffraction patterns were recorded using an ISO – DEBYEFLEX 2002 powder diffractometer employing a filtered Cu K_α (λ = 1 542 A) The generator was operated at 30 kV and 20 mA The scanning speed was 3°/min in 2θ

2 2 Thermal analysis

All the exothermic and endothermic transformations like melting, crystallization or phase transformations can be readily detected by thermal

analysis where the temperature of the sample is measured as a function of time

Thermal analysis in the temperature range – 500 ° C to 850 ° C was done for all the samples using a platinum crucible and Chromel – Alumel thermocouple The heating rate employed for the analysis was 15° C / min

2 3 Complex impedance analysis

DC measurements cannot be used to determine the DC resistance of ionic conductors because of polarization at the electrode – electrolyte interfaces The complex impedance analysis technique involves applying a low amplitude sinusoidal signal to the electrode - sample system

When a sinusoidal voltage of frequency, ϖ is applied to the system, the complex impedance at that frequency, $Z(\varpi)$is given by

$$Z(\varpi) = Z'(\varpi) + Z''(\varpi) \quad \text{---(2 1)}$$

where $Z(\varpi)$ and $Z''(\varpi)$ are real and imaginary parts of complex impedance respectively Or

$$Z(\varpi) = Z\exp(\theta) \text{---(2 2)}$$

where Z is the magnitude of complex impedance given by

$$Z = \left[(Z(\varpi))^2 + (Z''(\varpi))^2\right]^{1/2} \quad \text{--(2 3)}$$

And θ is the phase angle given by

$$\theta = \tan^{-1}\left(\frac{Z(\varpi)}{Z(\varpi)}\right) \quad -(2.4)$$

The electrochemical system of the leads electrodes and the solid electrolyte can be modeled using different combinations of resistors and capacitors The $Z(\varpi)$ Vs $Z(\varpi)$ plots for various representative circuits are described below

2.3.1 Pure Resistor

For a purely resistive circuit with resistance R the real and imaginary parts of complex impedance are given by

$$Z = R \quad Z = 0$$

The impedance plot i.e. the plot of Z Vs Z will be a point at $Z = R$

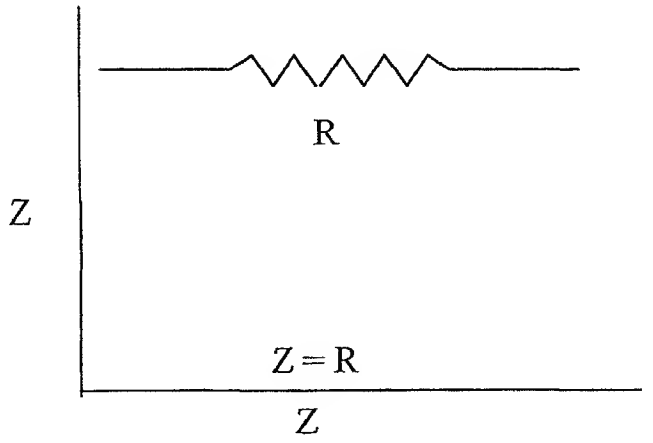

Figure 2.1(a) Impedance plot for a purely resistive circuit

2 3 2 Pure Capacitive circuit

For a purely capacitive circuit with capacitance C the real and imaginary parts of complex impedance are given by

$$Z' = 0 \quad Z'' = -1/\omega C$$

The impedance plot in this case will be a straight line parallel to negative Z axis at $Z' = 0$

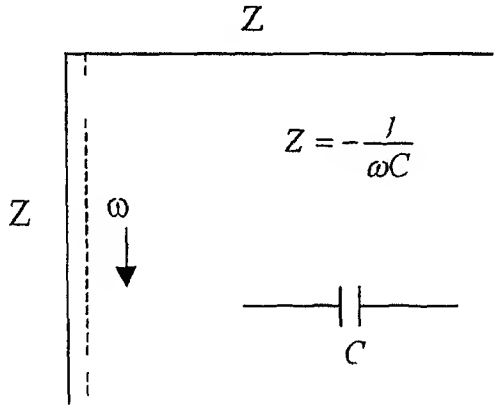

Figure 2 1(b) Impedance plot for a purely capacitive circuit

2 3 3 Resistor in series with a capacitor

For a series combination of a resistor R and a capacitor C the real and imaginary parts of complex impedance are given by

$$Z = R \quad Z = -1/\omega C$$

The impedance plot in this case is a straight line parallel to the negative Z axis at $Z = R$

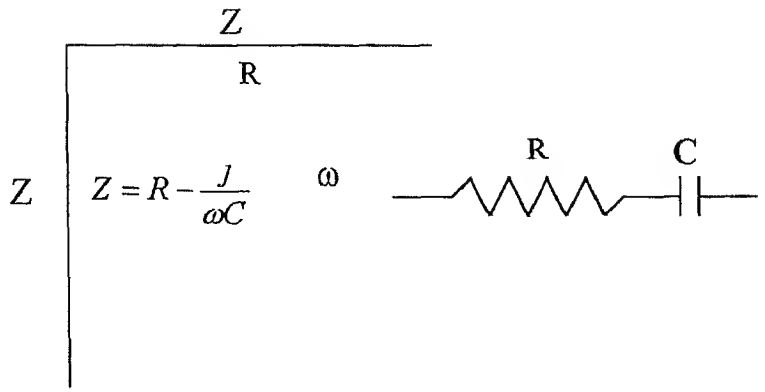

Figure 2 1(c) Impedance plot for a series combination of resistor and capacitor

2 3 4 Resistor in parallel with a capacitor

For a resistor R in parallel with a capacitor C, the complex impedance is given by

$$Z = \frac{R\left(\frac{1}{J\omega C}\right)}{R+\left(\frac{1}{J\omega C}\right)} \quad —(2\ 5)$$

The real and imaginary parts of impedance are given by

$$Z = \frac{R}{1+\omega^2 C^2 R^2} \quad —(2\ 6)$$

$$Z = \frac{\omega C R^2}{1+\omega^2 C^2 R^2} \quad —(2\ 7)$$

Eliminating frequency dependence from Equations *(2 6)* and *(2 7)* we have

$$Z^2 + Z^2 = RZ'$$

$$or \left(Z - \frac{R}{2}\right) + (Z'') = \left(\frac{R}{2}\right)^2 \quad —(2\ 8)$$

thus the impedance plot is expected to be a circle of radius *R 2* with center at *(R/2 0)*

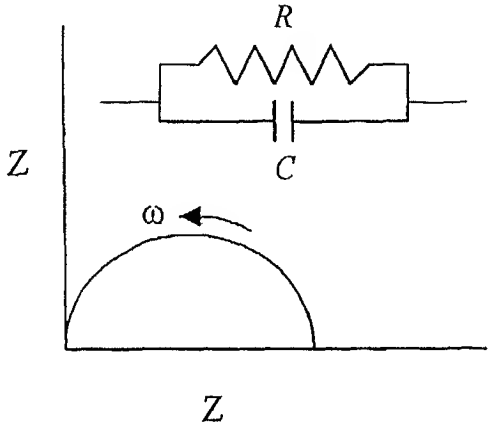

Figure 2 1(d) Impedance plot for a resistor and a capacitor in parallel

When electrodes different from the material of electrolyte are used for making the impedance measurements, apart from a semicircle, an inclined straight line, especially at lower frequencies, is also obtained The angle of inclination depends on smoothness of the surfaces This behavior is due to the interface capacitance C_{int} due to polarization at the electrode – electrolyte interface

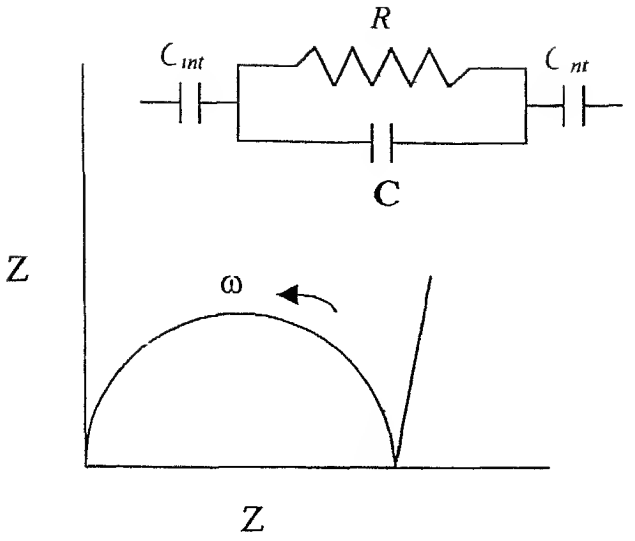

Figure 2 2(a) Effect of interface capacitance, C_{int} on the impedance plot

The impedance plot of a constant phase element connected in parallel with a resistor R is a depressed semicircle whose center lies below the positive Z' axis This behavior is shown by polycrystalline samples where multiple polarization is effective The resistor R in this case is the bulk resistance and the constant phase element is the capacitance due to multiple polarization CMP

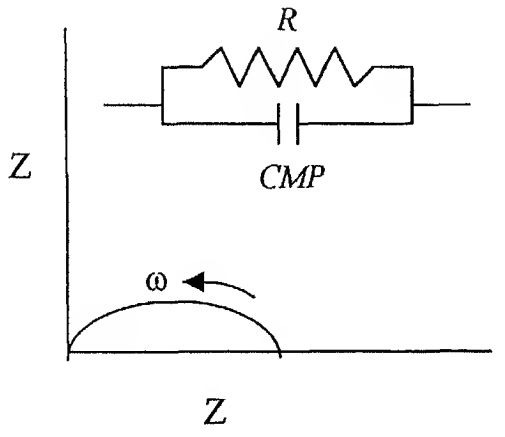

Figure 2 2(b) Depression of semicircle due to multiple polarization

Another phenomenon present in polycrystalline samples is the conduction through grain boundaries In such cases we obtain two semicircles The bulk resistance is obtained from the intersection of semicircle in high frequency regime with the positive Z axis

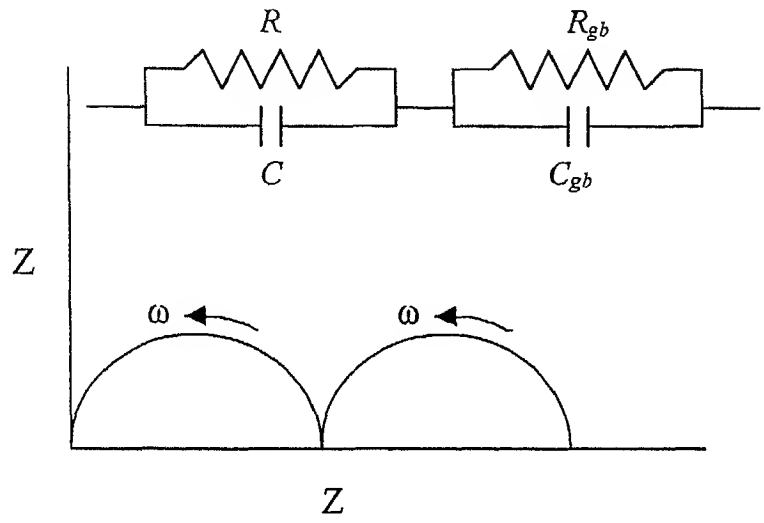

Figure 2 2(c) Effect of grain boundaries on the impedance plot

Complex impedance spectroscopy is a relatively simple technique that allows us to separate the contributions from various processes such as electrode reaction at electrode – electrolyte interface and the migration of charges through the grains and across the grain boundaries[24] Detailed analysis of the impedance data is possible by theoretically modeling an equivalent circuit The disadvantage of this technique lies in the fact that the equivalent circuit cannot be determined unambiguously

2 4 Experimental Set-up

2 4 1 Thermal Analysis

The block diagram of the experimental setup used for thermal analysis is shown in fig 2 3 The material to be analyzed is finely powdered and taken in a platinum crucible specially designed for thermal analysis A Chromel – Alumel thermocouple is used to measure the temperature of the sample The temperature of the sample is recorded as a function of time using a RISH Multi SI 232 data logger capable of recording one data point in 2 seconds The furnace is heated with a dimmerstat at 15°C/ min and cooled down using an INDOTHERM – 401 PID temperature controller at a rate of 5°C / min A special kind of sample holder has been designed to hold the sample, which is described in section 2 4 1 (a) All other equipments used are described in section 2 4 2

2 4 1 (a) Sample holder for thermal analysis

The sample holder consists of two lava discs of about 2 5 cm in diameter and 1 cm thick that have been sintered for hardening at 800°C for 8 hours after machining Each lava disc has 5 holes of 3 mm diameter, one at the center and 4 equally spaced along the periphery At the center of the lava discs, there is a depression 1 2 cm in diameter and 0 1 cm deep for holding the

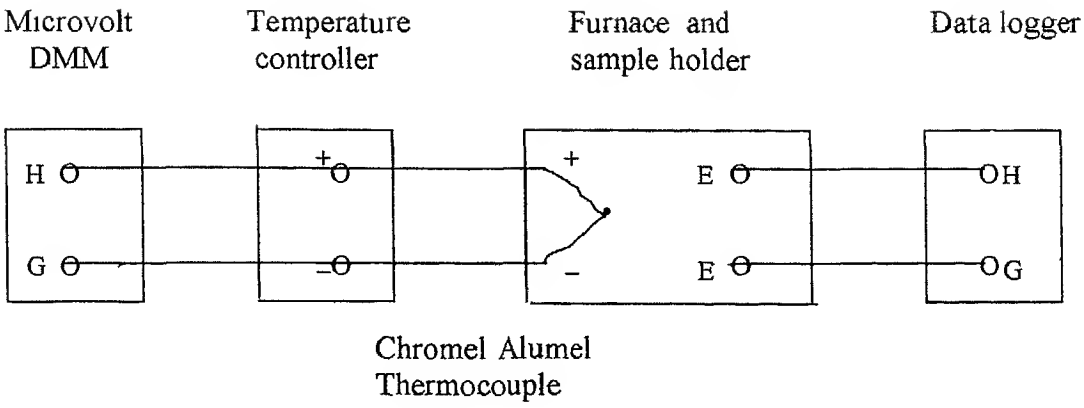

Figure 2 3 Block diagram of the experimental set-up used for thermal analysis

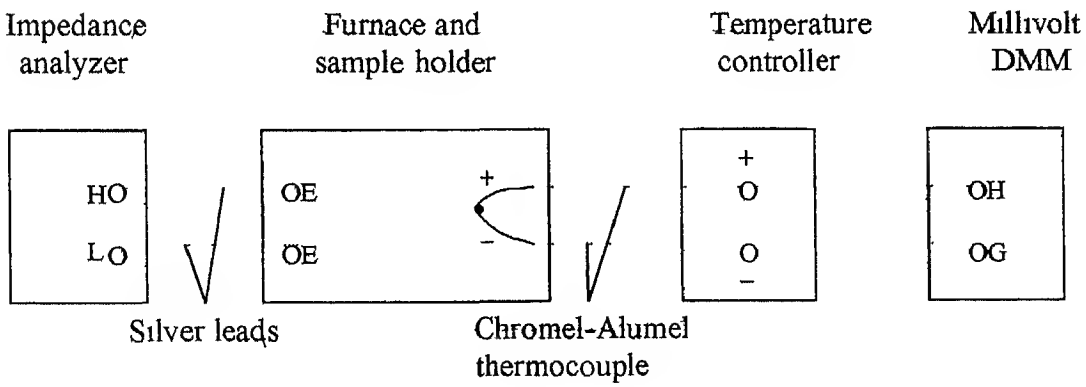

Figure 2 4 Block diagram of the experimental set-up used for conductivity measurements

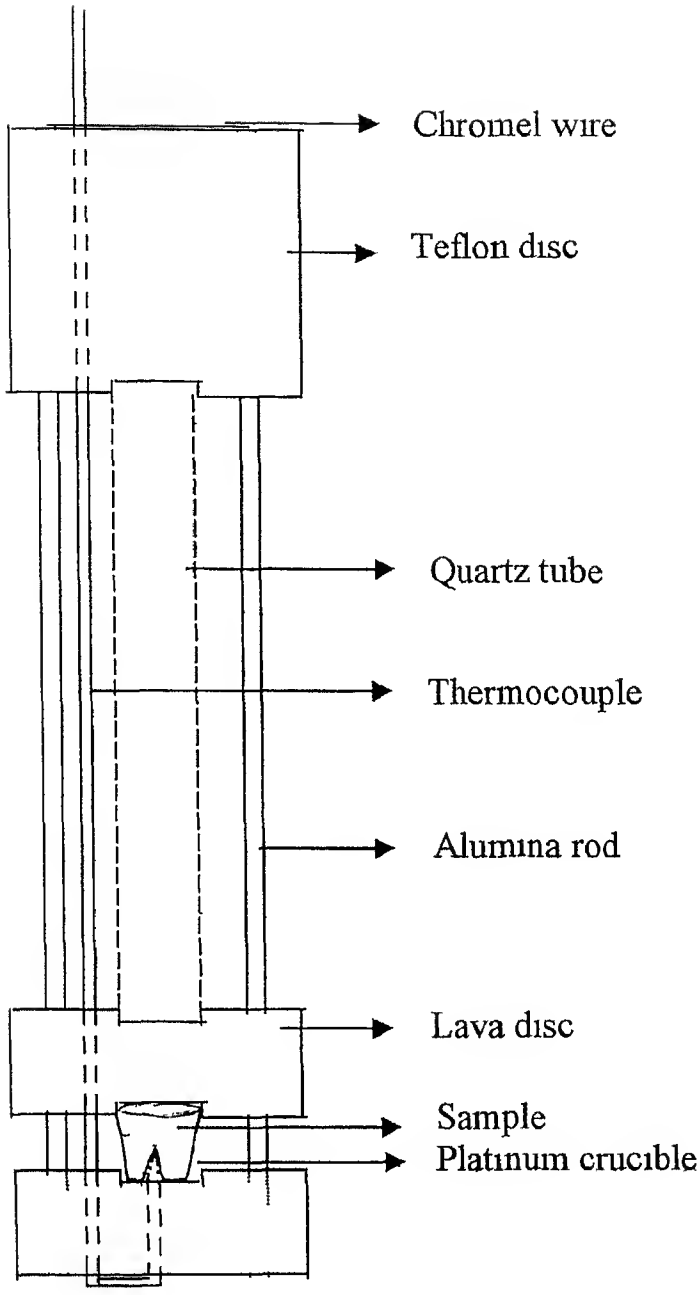

Figure 2 5 Sample holder for thermal analysis

platinum crucible Teflon disc 5 cm in length and 2 5 cm diameter with 4 holes equally spaced on the periphery was used to hold the sample holder on a stand Alumina rods were used to hold the crucible and the lava discs, with the help of a chromel wire, as shown in Fig 2 5 A thermocouple was placed as shown in the figure to measure the temperature of the sample

2 4 2 Complex impedance analysis

The block diagram of the experimental set-up used for complex impedance analysis is shown in Fig 2 4

The sample on which measurements have to be done is pelletized and mounted on a special kind of sample holder used for impedance analysis Chromel – Alumel thermocouple is used for measuring temperature of the sample The thermocouple voltage was measured using a KEITHLEY 197 autoranging microvolt DMM The furnace temperature was controlled using an INDOTHERM - 401 indicating temperature controller All the equipments used are described in detail below

2 4 2(a) Sample holder for complex impedance analysis

The sample holder used for complex impedance measurements is shown in Fig 2 6

It consists of 3 lava discs 2 5 cm diameter and 1 0 cm thick and Teflon disc 5 cm in length and 2 5 cm in diameter Each lava disc has 5 through holes of

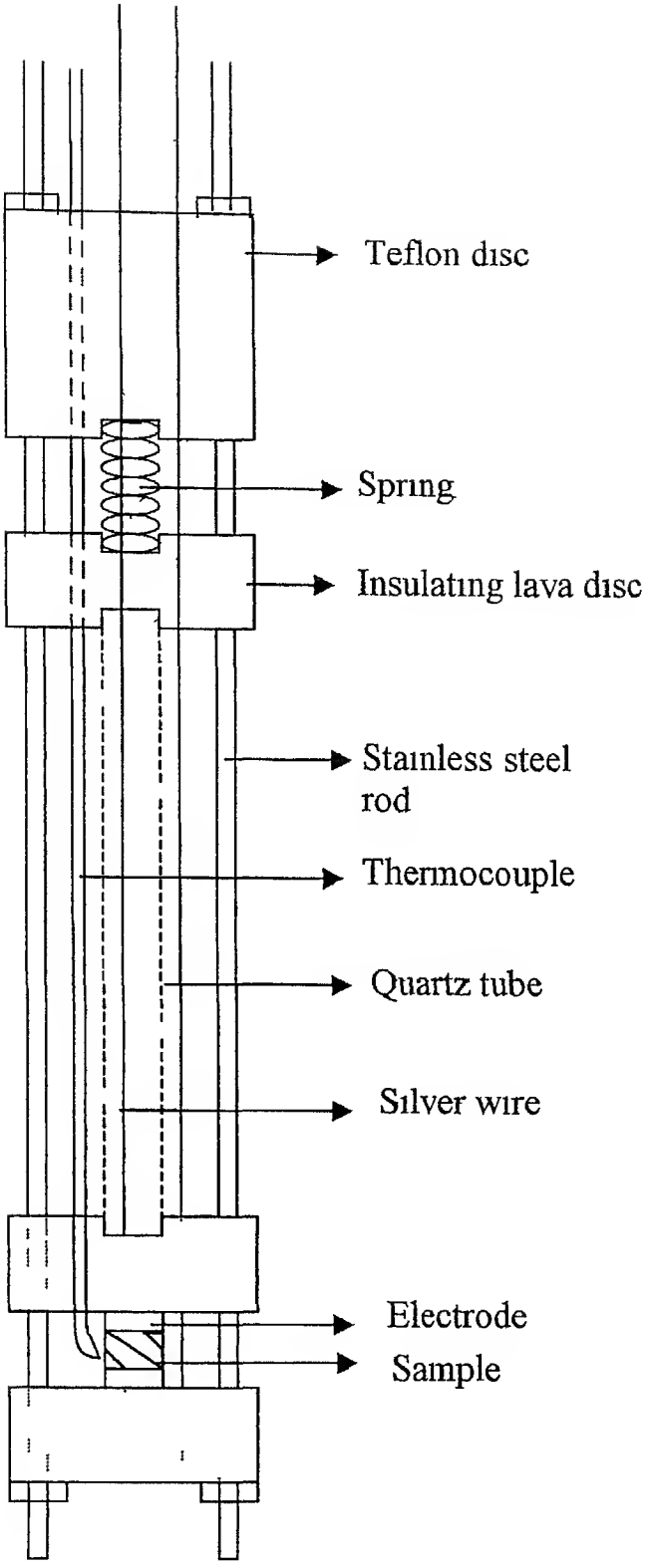

Figure 2 6 Sample-holder for complex impedance analysis

3 mm diameter in it, one at the center and 4 equally spaced along the periphery The sample pellet is placed between silver electrodes that are brazed using brass with silver wires The silver wires are taken out through the holes in the lava discs as shown in the figure These 2 lava discs are separated from the other end of the sample holder by a quartz tube 16 cm long and 1 2 cm diameter A stainless steel compression spring placed between the lava disc and the teflon disc helps to hold the sample pellet intact, which ensures proper contact between the electrodes and the sample The spring and the teflon disc are always at room temperature The entire arrangement is held intact with the help of stainless steel rods threaded and bolted tightly at both the ends as shown in Fig 2 6 One of the holes along the periphery of the lava discs is used to hold the thermocouple close to the pellet as shown in Fig 2 6

2 4 2 (b) Furnace and temperature controller

An electrical heating furnace with kanthal winding has been used in the set – up The furnace comprises of a mullite tube of inner diameter 4 cm High temperature cement applied over the kanthal winding keeps it intact in its place The mullite tube with cemented kanthal wiring is enveloped with a cylindrical aluminium container and the annular space between the two is filled with MgO powder for heat insulation

An INDOTHERM 401 PID temperature controller has been used to control the heating rate of the furnace A platinum – 13 % rhodium thermocouple has been used for providing feedback to the temperature controller

2 4 2(c) Impedance Analyzer

Impedance analyzer is a small - signal ac measurement device with a wide range of frequencies to investigate the electrochemical properties of the solid electrolytes A HP 4192 A impedance analyzer has been used in the set – up The instrument has an autobalancing bridge with a test signal from 5 mV to 1 1 V One can sweep the frequency from 5 Hz to 13 MHz The two displays A' and B display the associated pairs such as

Table 2 1 The displays 'A' and 'B' of the impedance analyzer

A	B
complex impedance (Z) admittance (Y)	phase angle (θ) (degrees or radians)
resistance (R) conductance (G)	reactance (X)
inductance (L) capacitance (C)	Q – factor D – value

One can select any pair of interest in either series or parallel mode.

2 5 Materials Processing

The physical and chemical properties of the starting materials viz NaF and NaBr- are summarized in Table 2 2

Table 2 2 Physical and chemical properties of starting materials

properties	NaF	NaBr
source	Reanal Chemicals	Aldrich Chemicals
purity	-	99+%
molecular weight	41 99	102 90
melting point (Celsius)	993	747
boiling point (Celsius)	1695	1390
density (kg/m^3)	2558	3203
Bravais lattice	cubic or tetragonal	cubic

The appropriate quantities of NaF and NaBr for each composition to be analyzed were weighed using an Afcoset ER–120A electronic balance They were then mixed thoroughly by mechanical grinding using a mortar and pestle The mixture was transferred into a quartz crucible and then heated to 850°C (temperature greater than melting point of all compositions) The temperature was maintained at 850°C for about half an hour for homogenization of the sample The melt was then allowed to cool down slowly at the rate of 5-10°C/min It was again pulverized finely A part of

the rest was pelletized using a hydraulic press A pressure of 4 tons was always used for pelletization All the pellets were sintered properly at appropriate temperatures (~ 2/3 of melting point) for elimination of pores The pellet thickness and sintering time for all compositions are listed in Table 2 3 Diameter of pellets was 1 1 cm

Table 2 3 Processing parameters for various compositions

composition	thickness of pellet (in mm)	sintering time (in hours)
NaF	3 40	9
NaF+*1 m/o*NaBr	3 10	9
NaF+*2 m/o*NaBr	3 8	9
NaF+*3 m/o*NaBr	2 5	9
NaF+*5 m/o*NaBr	4 40	9
NaF+*10 m/o*NaBr	3 34	9
NaF+*20 m/o*NaBr	2 20	9
NaF+*30 m/o*NaBr	2 20	9
NaF+*40 m/o*NaBr	2 80	9
NaF+*50 m/o*NaBr	3 00	9
*40 m/o*NaF+NaBr	2 36	9
*30 m/o*NaF+NaBr	2 90	9
*20 m/o*NaF+NaBr	3 30	9
*10 m/o*NaF+NaBr	2 58	9
*5 m/o*NaF+NaBr	2 46	9
NaBr	2 40	9

The pellets were coated with conducting graphite paint on both sides and were allowed to dry The resistance of the graphite paint electrodes was ~50 Ω The pellets were then loaded on the sample holder for conductivity measurements All the measurements were repeated twice to test the reproducibility of results

Chapter 3

Results and Discussion

With an intention to determine the maximum enhancement in the conductivity as a function of dopant concentration sixteen different compositions of the NaF-NaBr mixed crystal system have been prepared and analyzed XRD-measurements have been carried out for structural analysis They have been useful in identifying the different phases present in the system Thermal analysis has been done to determine the various phase transition temperature(s) present in the NaF-NaBr system Complex impedance data were taken to extract AC/DC conductivities for different systems as a function of temperature The activation energies in different temperature regimes and the temperature at which there is a transition from extrinsic to intrinsic behavior for all compositions have been determined using the complex impedance analysis data In addition to the above mentioned results results on conductivity vs composition are also presented in this chapter

3 1 X-ray Diffraction

From the data available in literature[26], it has been found that NaBr has a cubic Bravais lattice, where as NaF has either cubic or tetragonal Bravais lattice The results obtained from XRD studies and the corresponding data available in literature are summarized in Table 3 1

Table 3 1 Bravais lattice and lattice parameter of the starting materials

	Bravais lattice[26]	Bravais lattice (experimental)	lattice parameter[16] (A)	lattice Parameter(A) (experimental)
NaF	cubic/ tetragonal	cubic*(FCC)*	4 63329	4 64
NaBr	cubic	cubic*(FCC)*	5 97353	5 96

The XRD patterns of NaF NaBr and two samples of intermediate compositions viz NaBr+*30m/o*NaF and NaF+*30m/o*NaBr are shown in Figs 3 1a - d respectively

The XRD patterns of all the compositions from NaF+*5m o*NaBr to NaF+*95m/o*NaBr show the peaks corresponding to both pure NaF and NaBr though with slight variations in the intensities This suggests that at room temperature there are two distinct phases present in all the samples The two phases are solid solutions of NaF in NaBr and of NaBr in NaF The variation in the relative intensities of the various peaks may be attributed to the changes in the composition of the samples

XRD patterns of NaF+*1m/o*NaBr, NaF+*2m o*NaBr and NaF+*3m/o*NaBr do not show any peak corresponding to pure NaBr There is a shift in the position of the peaks corresponding to pure NaF towards higher 2θ values This suggests that the lattice parameter has decreased The calculated values of lattice parameters are listed in Table3 2

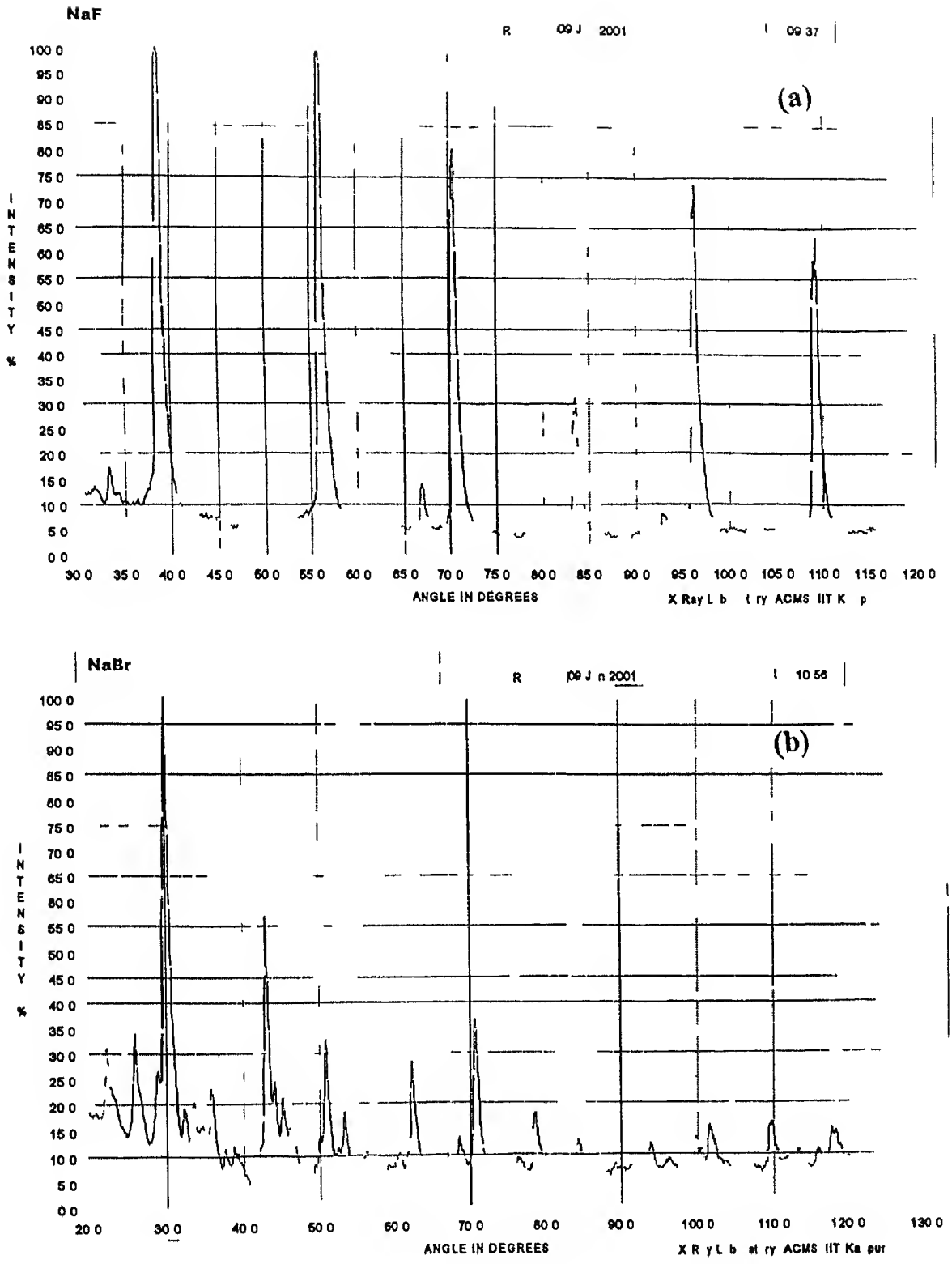

Figure3 1 XRD pattern for (a) NaF , (b) NaBr

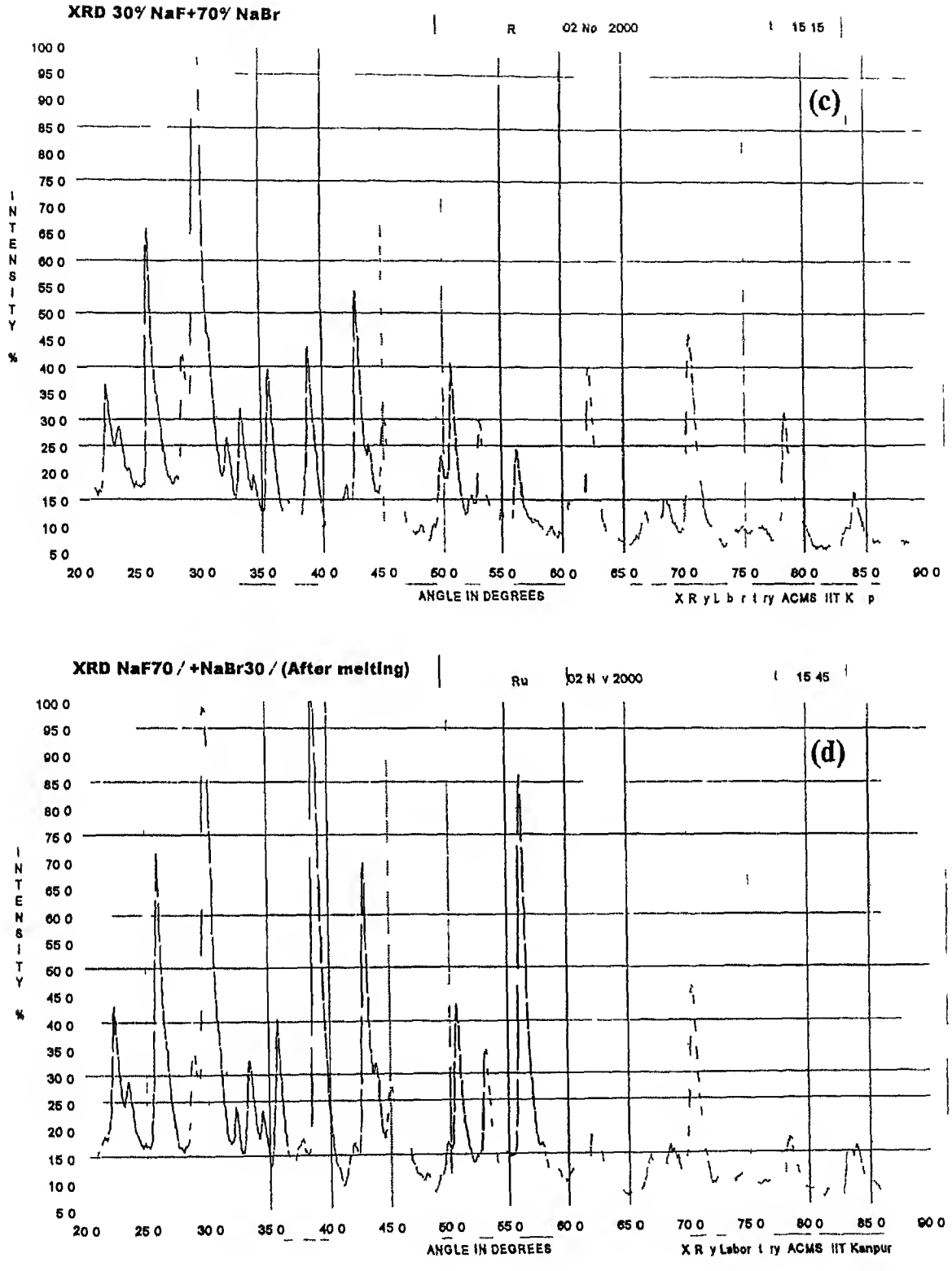

Figure3 1 XRD pattern for (c) NaBr+*30m/o*NaF, (d) NaF+*30m/o*NaBr

XRD pattern of NaBr+*1m o*NaF does not show any peak corresponding to pure NaF It shows peaks corresponding to pure NaBr that have shifted towards lower 2θ values This suggests an increase in the lattice parameter The calculated lattice parameters are listed in Table 3 2

Table3 2 calculated values of lattice parameters for different systems

system	lattice parameter (A)	Bravais lattice
NaF	4 64	cubic
NaBr	5 96	cubic
NaF+*1m/o*NaBr	4 62	cubic
NaBr+*1m/o*NaF	5 97	cubic

The peak positions and their relative intensities used for determining the lattice parameters (Table 3 2) are listed in Table 3 3

As pointed out earlier, the XRD patterns of NaF+*2m/o*NaBr and NaF+*3m/o*NaBr do not show any peaks corresponding to NaBr and the existing peaks appear at the same positions (within the limits of experimental errors) as those of NaF+*1m/o*NaBr This clearly suggests that the maximum concentration of NaBr that goes into solid solution with NaF is nearly *1m/o* The absence of peaks corresponding to NaBr may be due to very low concentration of the dopant

Table 3 3 Peak positions and the corresponding relative intensities, used in calculating the lattice parameters

NaF peak position (2θ)	NaF relative intensity	NaF +1m/o NaBr (2θ)	NaF +1m/o NaBr relative intensity	NaBr (2θ)	NaBr Relative intensity	NaBr+ 1 m/oNaF (2θ)	NaBr + 1m/oNaF relative intensity
38 53	100 00	38 85	99 95	30 04	100 00	29 90	100 00
55 93	99 55	56 47	98 71	42 95	56 23	42 95	43 61
70 34	80 51	70 84	30 55	53 24	18 45	53 14	18 05
83 43	31 15	83 88	19 14	62 29	27 84	62 16	38 07
96 08	70 88	96 48	51 08	70 65	36 25	70 51	25 55
109 22	62 95	109 42	33 12	-	-		-

It is interesting to note that the lattice parameter of NaBr increases, though nominally (by 0 17%) due to doping with smaller size anions (F) whereas the lattice parameter of NaF decreases (by 0 43%) due to doping with larger size anions (Br)

The increase in the lattice parameter of NaBr due to doping with an anion of smaller ionic radius suggests that the fluoride ions might go into the interstitial sites, thus leading to an increase in the concentration of anion vacancies

3 2 Thei mal analysis

In oidei to corielate the observed conductivity vs composition data to the diffeient phases piesent in the system attempts have been made to construct the phase diagiam for the binary system NaF-NaBr

At a constant heating rate of 15°C/min the temperature of the sample was recorded as a function of time for all compositions The heating rate was decided by calibrating against pure compounds like NaBr and Li_2SO_4 Fig 3 2 shows some representative plots All the temperature vs time plots show diviation from linearity at certain temperatures indicating that certain phase transitions occur at these temperatures

Figure 3 3 depicts the phase diagram for the NaF-NaBr system which has been constructed using the thermal analysis data The eutectic temperature as determined experimentally is ~640°C The experimental data compares well with the data available in literature[27]

The theoretical best fit curves for the experimentally obtained data shown in Fig 3 3 are given by the following equations

Hypo-eutectic composition

$$T = 989 - 3\,1x - 0\,02x^2 \quad - \quad (3\ 1)$$

Hyper-eutectic composition

$$T = 520 + 0\,06x + 0\,022x^2 \quad - \quad (3\ 2)$$

where T is the temperature in °C and x is the composition (*m/o* NaBr)

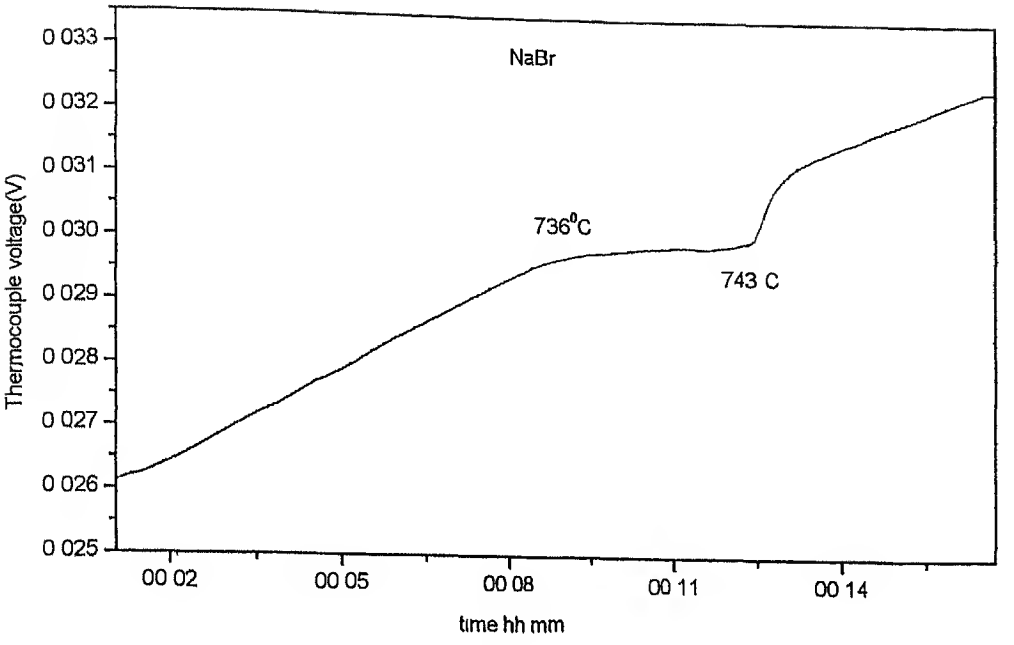

(a)

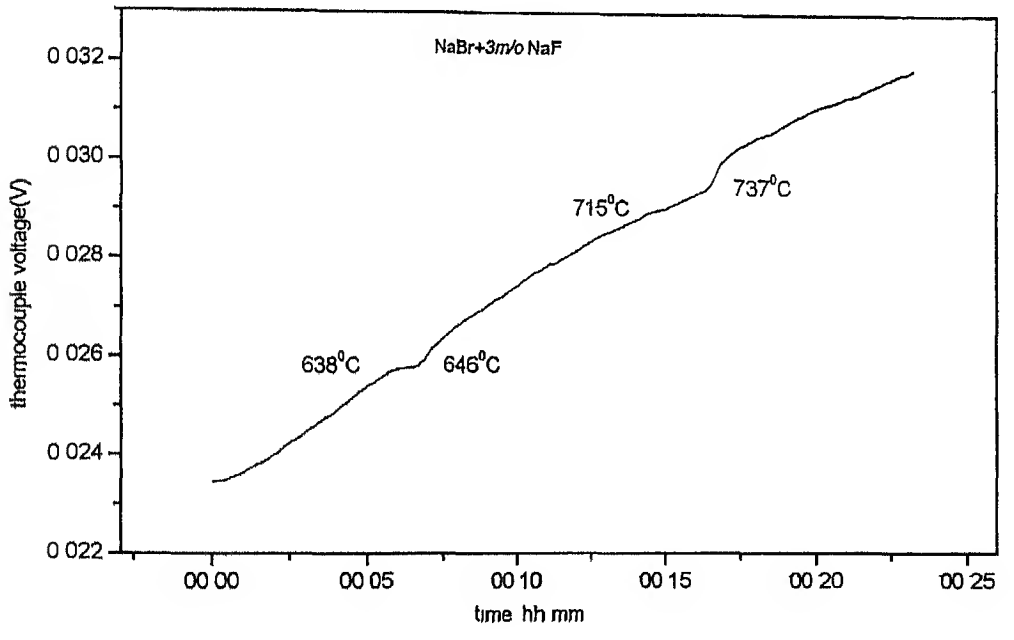

(b)

Figure 3 2 Typical thermal analysis data for pure NaBr (a) and NaBr+*3m/o* NaF (b) The actual transition temperatures were obtained by taking the average of temperatures corresponding to the onset and completion of the transition

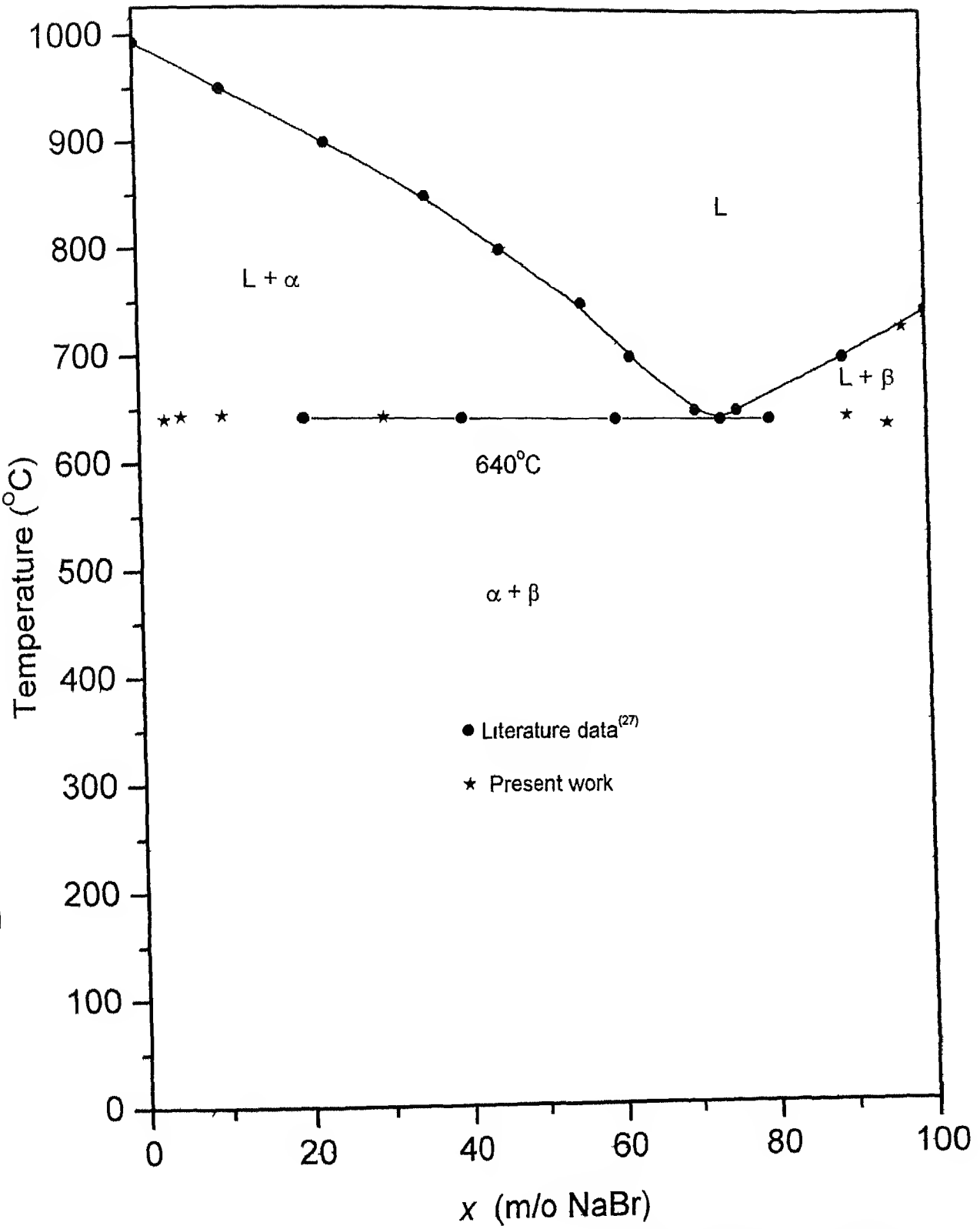

Figure 3 3 Phase diagram for the NaF NaBr binary system

α **NaF+1m/o NaBr**

β **NaBr containing small amount of NaF**

3 3 Complex impedance analysis

The dc conductivity at different temperatures was calculated for all the samples from the experimentally obtained complex impedance data The variation of real and imaginary parts of complex impedance as a function of frequency has been used to calculate the dc resistance Fig 3 4 shows the variation of real and imaginary parts of complex impedance as a function of frequency at four different temperatures for NaF

Similar plots were obtained in case of all samples (NaF+*xm/o*NaBr *x = 0 1 2 3 5 10 20 30 40 50 60 70 80 90 95 100)* As observed in fig (3 4) we obtain good semi circles (within the limits of experimental error) suggesting that the sample/electrode assembly behaves like a parallel combination of a resistor and a capacitor The dc resistance in this case is thus given by the diameter of the semi-circle

The dc conductivities obtained as described above have been plotted against inverse absolute temperature for all the sixteen samples Fig 3 5 shows some typical log(conductivity) vs 1/T plots However, the ionic transport parameters (knee temperature, extrinsic activation-energy and intrinsic activation-energy) for all the studied compositions are summarized in Table 3 4

All the plots show that the logarithm of conductivity varies linearly with inverse temperature, with two distinct slopes in the (low temperature) extrinsic region and the (high temperature) intrinsic region The activation

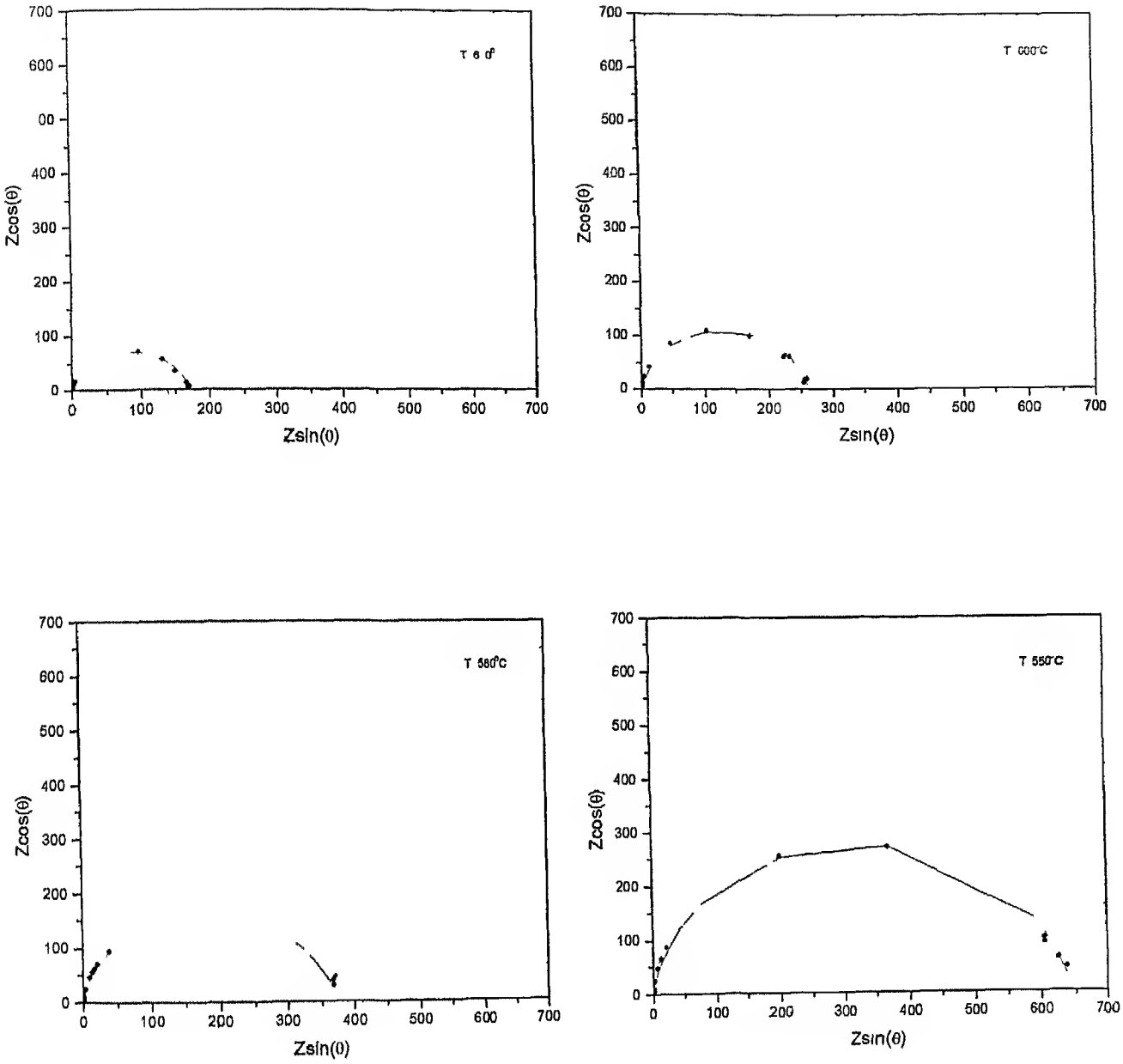

Figure 3 4 Variation of real and imaginary parts of complex impedance as a function of frequency at four different temperatures for NaF

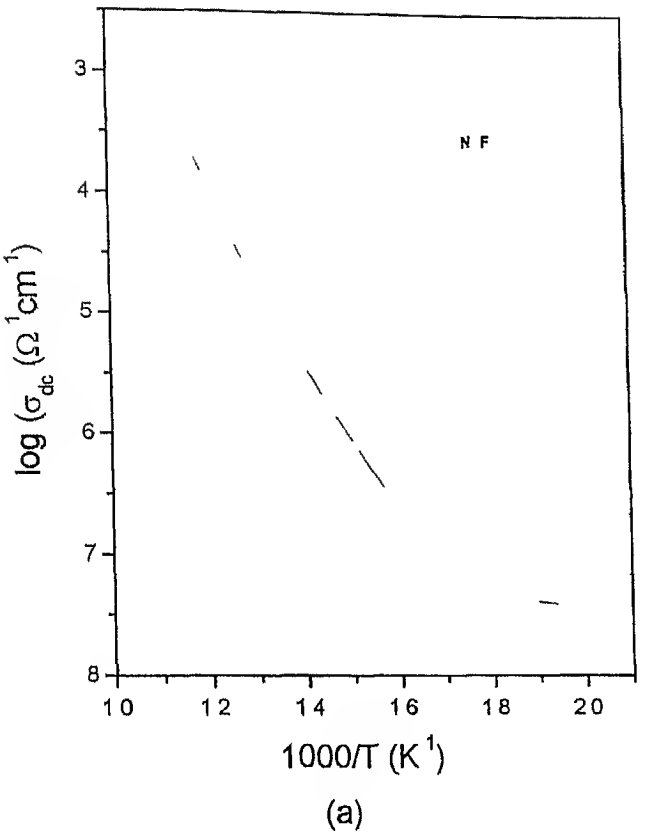

(a)

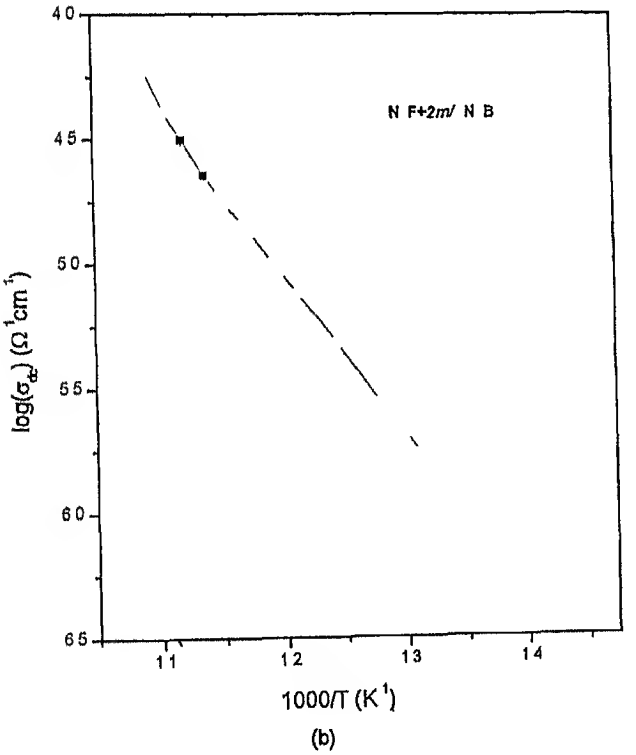

(b)

Figure 3 5 log(conductivity) vs inverse absolute temperature for (a) NaF and (b) NaF+2*m*/oNaBr)

energies in the two temperature regimes have been calculated for all the samples Table 3 4 lists the knee temperature (temperature at which there is a transition from extrinsic to intrinsic behaviour) and the activation energies in the intrinsic and extrinsic regions for all the samples studied

Table 3 4 Knee temperature and the activation energies in the intrinsic and extrinsic regions for various compositions in the NaF-NaBr system

composition	knee temperature (K)	activation energy (intrinsic region) (eV)	activation energy (extrinsic region) (eV)
NaF	901	2 76	1 19
NaF+*1m o*NaBr	870	2 54	1 01
NaF+*2m/o*NaBr	821	1 25	1 03
NaF+*3m/o*NaBr	826	1 10	1 06
NaF+*5m/o*NaBr	820	2 53	0 85
NaF+*10m/o*NaBr	840	1 96	0 99
NaF+*20m/o*NaBr	820	1 63	1 22
NaF+*30m/o*NaBr	855	2 94	1 27
NaF+*40m/o*NaBr	870	1 32	0 94
NaF+*50m/0*NaBr	840	1 48	1 00
NaBr+*40m/o*NaF	870	1 33	0 93
NaBr+*30m/o*NaF	877	1 94	0 97
NaBr+ *20m/o*NaF	870	1 53	0 90
NaBr+*10m/o*NaF	862	2 15	0 96
NaBr+*5m/o*NaF	816	1 92	0 96
NaBr	893	1 56	1 05

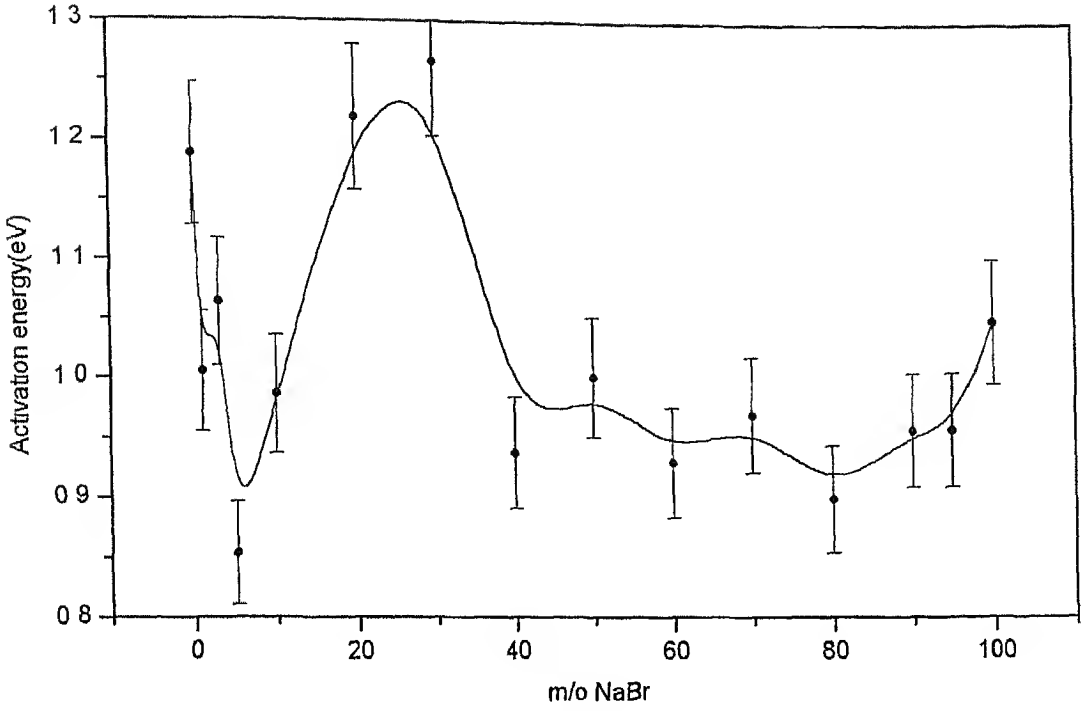

(a)

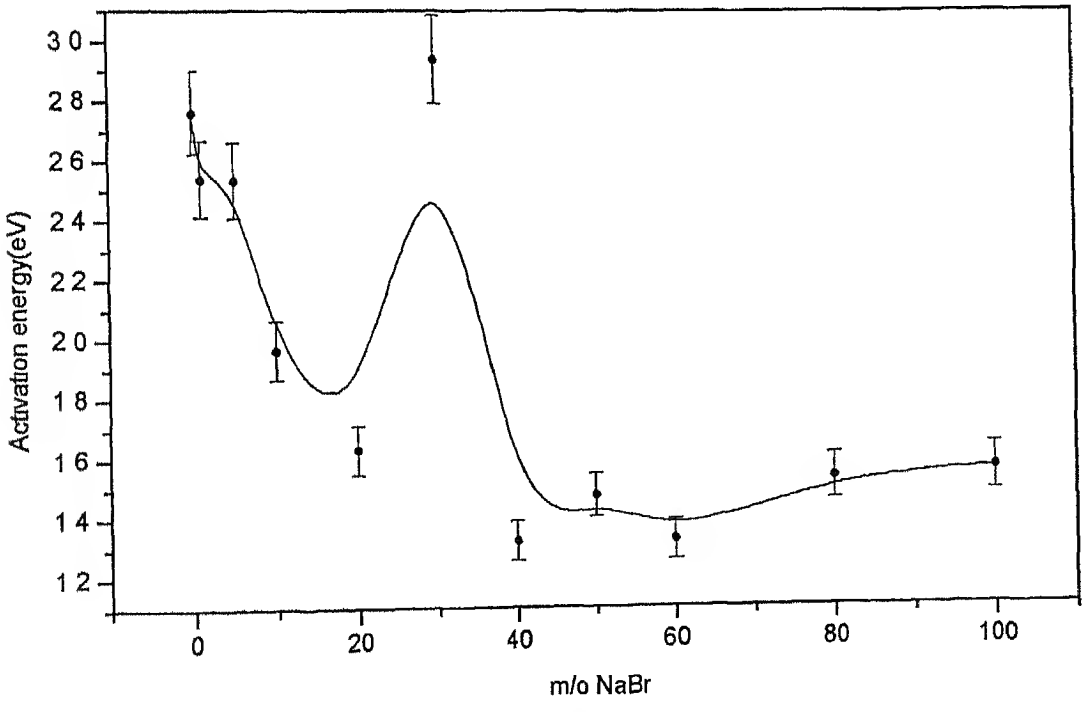

(b)

Figure 3 6 Variation of activation energy as a function of composition, in both the extrinsic region (a) and the intrinsic region (b)

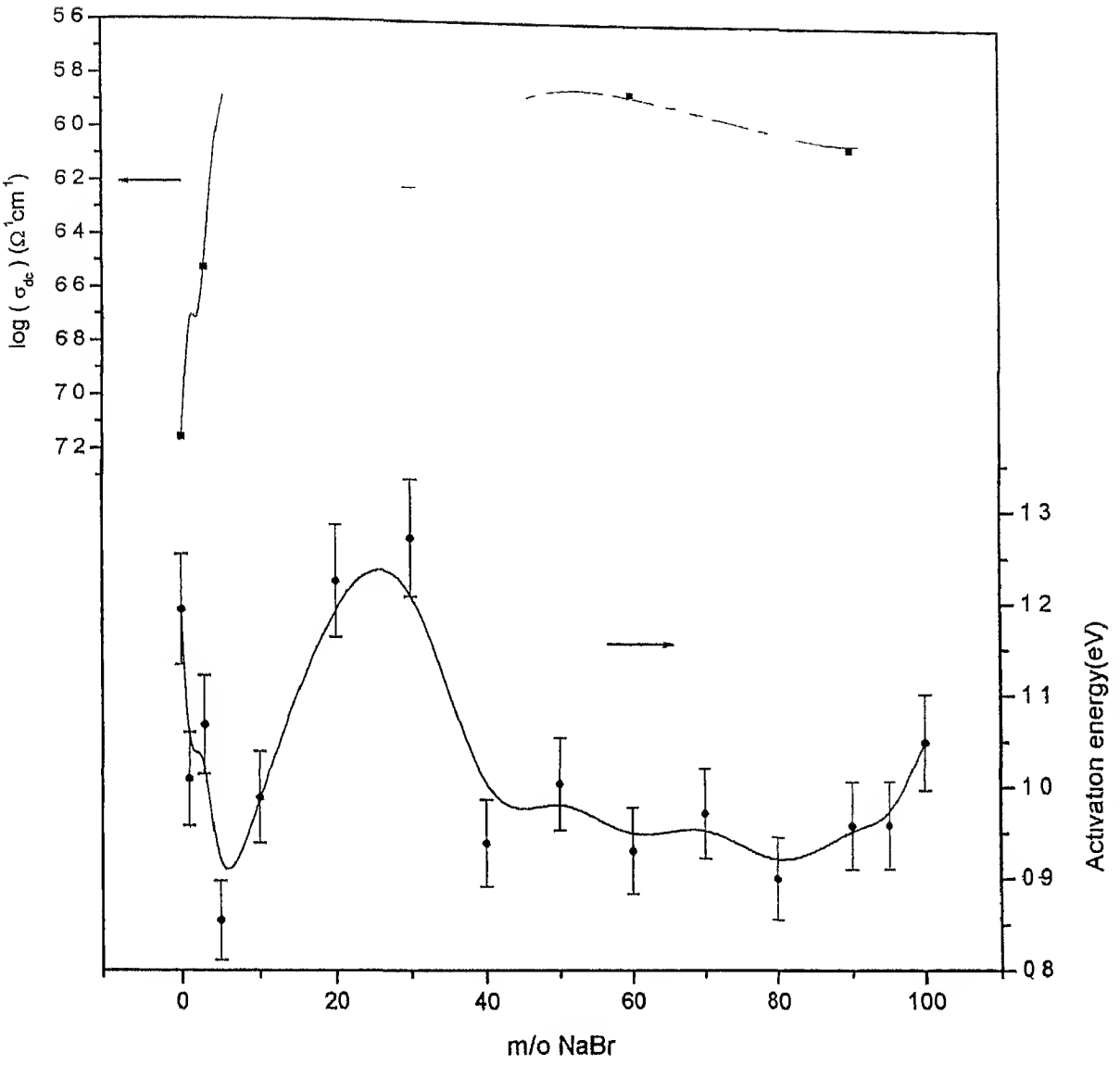

Figure 3 7 variation of activation energy in the extrinsic region and the conductivity isotherm at 393°C

Figure 3 6 shows the variation of activation energy as a function of composition in both the extrinsic and the intrinsic regions The conductivity isotherms at 393°C (lying in the extrinsic region for all the compositions studied) and 870°C (lying in the intrinsic region for all the compositions studied) are shown in Figs 3 7 and 3 8 respectively

In the extrinsic temperature regime doping with *1m/o*NaBr reduces the activation energy of NaF from 1 19 eV to 1 01 eV (Fig 3 6) The activation energy then remains constant as the dopant concentration increases upto *3m o* However, the *5m/o*NaBr doped NaF shows further decrease in activation energy (0 85 eV) The activation energy then increases with further increasing dopant concentration exhibiting a local maximum at a composition of *~30m/o*NaBr The activation energy practically remains constant for the composition range NaF+*xm o*NaBr $40 \leq x \leq 95$ and then increases to 1 05 eV for pure NaBr

The activation energy in the intrinsic temperature regime (Fig3 6 (b)) shows a similar behavior The activation energy first decreases from 2 76 eV for pure NaF to 2 54 eV for *10m/o*NaBr doped NaF There is a local maximum in the activation energy plot at 2 94 eV corresponding to NaF+*30m o*NaBr

Figs 3 7 and 3 8 show that the conductivity isotherms show a trend similar to the activation energy plots but in the opposite sense The conductivity isotherms exhibit a maximum at *5m/o*NaBr and a minimum at *30m/o*NaBr as expected from the behaviour of the activation energy vs composition plots The maximum conductivity, corresponding to NaF+*5m o*NaBr is $1\ 78\times10^{-6}\ \Omega^{-1}cm^{-1}$ at 393°C and $7\ 8\times10^{-4}\ \Omega^{-1}cm^{-1}$ at 870°C

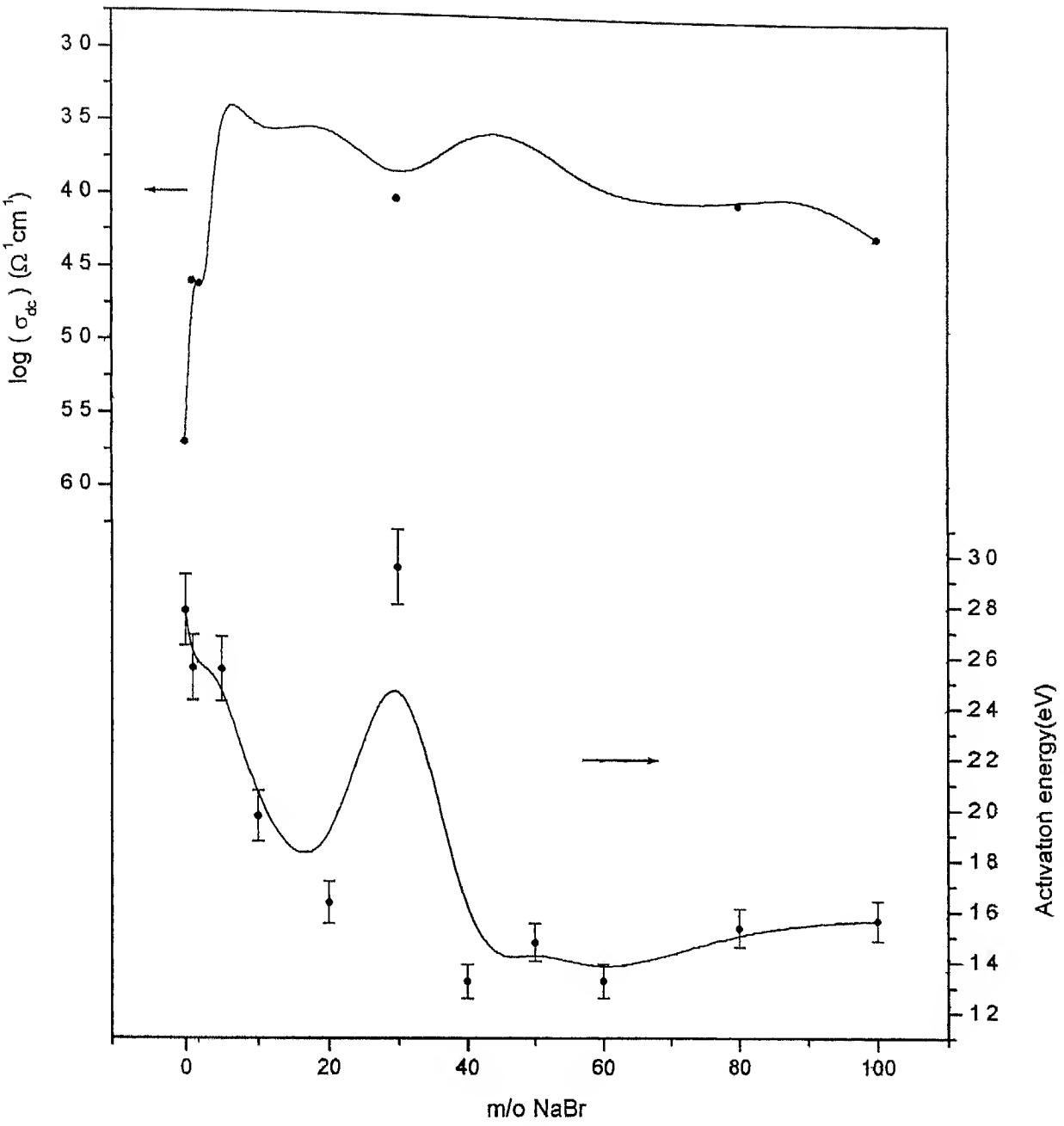

Figure 3 8 Variation of activation energy in the intrinsic region and the conductivity isotherm at 870°C

All the above experimentally observed features can be explained using the lattice loosening[19] model in the solid solution region and the percolation model[24] in the two phase region

Lattice–loosening model predicts an increase in conductivity in the solid solution region, for a homovalently doped salt due to strains produced in the lattice because of mismatch in the sizes of the host and the dopant ions It states that the increase in conductivity varies exponentially with decrease in the melting point of the salt upon doping According to the lattice loosening model the relative conductivity varies exponentially with inverse absolute temperature (Eqn 1 26) The experimentally observed value for the relative conductivity of NaF+*1m/o*NaBr is 3 at 400°C Using Eqn 1 26 the expected decrease in melting temperature is 13°C From the theoretical fit (Eqn 3 1) for the liquidus in Fig 3 3, the liquidus temperature for NaF+*1m/o*NaBr is 989 5°C Thus the change in liquidus temperature is only 3 5°C The slight mismatch between the ΔT_M values calculated from the experimental data and from the phase diagram can be attributed to the experimental errors and the various approximations used in deriving Eqn 1 26

It has been earlier reported by Manoravi[28] that the enhancement in conductivity of a mixed crystal in the solid solution region, with respect to the pure component varies exponentially with the change in solidus temperature The binary systems studied in this case were NaBr NaCl and NaBr-NaI Both these systems exhibit solid solution over the entire composition range and the maximum difference between the solidus and liquidus temperatures in either case was ~10 15°C With such a small difference between the solidus and liquidus temperature, it cannot be

decisively concluded that change in solidus temperature rather than the liquidus temperature is the determining factor for increase in conductivity In the NaF-NaBr binary system, the solidus and liquidus temperatures for NaF + *1m/o*NaBr differ by 350°C Substituting the decrease in solidus temperature for ΔT_M in Eqn 1 26, enhancement in conductivity by 5 orders of magnitude are expected for NaF+*1m/o*NaBr with respect to the conductivity of pure NaF whereas substituting the decrease in liquidus temperature for ΔT_M in Eqn 1 26, enhancement in conductivity by a factor of 2 for NaF+*1m/o*NaBr with respect to the conductivity of pure NaF is expected at a temperature of 390°C The experimentally observed value of relative conductivity at the same temperature and composition is 3 This suggests that the enhancement in the conductivity is exponentially dependent on the decrease in liquidus temperature, rather than the decrease in solidus temperature

The variation of activation-energy as a function of composition and the conductivity isotherms in the composition range *1-5m/o*NaBr can be explained using the percolation model[24] The percolation model states that in a two-phase mixed crystal system, there exists a minimum concentration of the dopant, the percolation threshold, until which there is no enhancement in the conductivity of the system The percolation threshold corresponds to the minimum concentration at which there is a continuum of the charged double layer formed. The percolation threshold should obviously depend on the grain size, which depends on the cooling rate From the conductivity isotherms (Fig 3 7) the percolation threshold for NaBr dispersed in NaF mixed crystal system is achieved for a composition between *3* and *5m/o*NaBr doped NaF The cooling rate employed in this case was 5-10°C/minute

Further studies with samples prepared under controlled cooling rate will be required to determine the percolation threshold precisely The minimum in the activation-energy vs composition plots (Fig 3 6) and the maximum in the conductivity isotherms (Fig 3 7) that are observed at NaF+5*m* oNaBr can be attributed to the formation of a continuous charged double layer, beyond the percolation threshold

The enhancement in the conductivity in the two-phase region is due to the formation of a double layer rich in defects at the grain boundaries where two dissimilar phases come into contact with each other[22] The conductivity of this double layer at the interfaces is supposedly greater than that of either of the phases present in the system At very low concentrations of the second phase particles, the conductivity of the system does not change inspite of the formation of the double layer because of the lack of continuous channels for migration of the defects As mentioned earlier the critical concentration required for the formation of a continuous double layer is the percolation threshold As the concentration of the second phase increases beyond the threshold, the second phase particles might not contribute to the formation of additional interfacial regions, but might increase the thickness of the second phase around the double layer Since the second phase has a lower defect concentration than the double layer the conductivity of the system decreases The local minimum at *30m*oNaBr in the conductivity isotherms may be due to the increase in the thickness of β -phase (NaF solid solution with NaBr) around the double layer

One of the motivations behind choosing the NaF-NaBr system for this work was the large mismatch in the ionic radii of the host and the dopant ions,

thus expecting a large enhancement in the conductivity The mismatch factor and the observed enhancement in the conductivity at 600°C for various systems are reported in Table3 5

Table 3 5 The mismatch factor and the maximum enhancement in conductivity at 600°C for various systems

system	mismatch-factor $\left\|1-\frac{r_d}{r_h}\right\|$	x_m (m/o NaBr)	maximum relative conductivity (at x_m)
NaCl NaBr[28]	0 08	60	5
NaI-NaBr[28]	0 11	30	15
NaF-NaBr	0 47	1	4

The conductivity of NaF is increased by a factor of 4 at 600°C by doping with just *1m/o*Br The total enhancement in the conductivity for Br doped NaCl and NaI is by a factor of 5 and 15 respectively, at a dopant concentration of *60* and *30m/o* respectively It is interesting to note that eventhough the total enhancement in conductivity for the NaF-NaBr system is low, the conductivity enhancement per *m o* dopant is very high in comparison to the other two systems listed in Table 3 5 This feature is well understood in light of large mismatch factor (~ 47 %) in the radii of the host and the dopant ions in the NaF-NaBr system Unfortunately only about *1m/o*NaBr goes into solid solution with NaF, thus limiting the conductivity

enhancement to a factor of four at 600°C Large enhancement would have been possible if there was solid solution formed for higher dopant concentrations

Chapter 4

Conclusions

The conductivity of NaF increases by more than an order of magnitude at 800°C due to doping with NaBr inspite of the fact that the solid solubility is limited to just *1m/o* The conductivity enhancement per *m/o* dopant in the NaF-NaBr system is very high in comparison to NaCl NaBr[28] and NaI-NaBr[28] systems This feature is well explained using the lattice-loosening model[19] in light of large mismatch factor (~ 47%) in the radii of the host and the dopant ions in the NaF NaBr system

The difference between the change in solidus temperature and the liquidus temperature for NaF+*1m/o*NaBr is ~350°C This difference is very large compared to the difference in solidus and liquidus temperatures for other systems like NaCl doped with NaBr and NaI doped with NaBr thus enabling to conclude that the decrease in liquidus temperature rather than the decrease in solidus temperature decides the magnitude of conductivity enhancement

The conductivity measurements for binary systems in the solid solution region can be used to predict the liquidus temperature for various compositions through Eqn 1 26

)

The conductivity of NaF increases by more than an order of magnitude due to doping with NaBr in the solid solution region The conductivity then practically remains constant till NaBr concentration increases to *3m/o* Sudden increase in conductivity is observed at *5m o*NaBr Percolation model[24] predicts the existence of a critical concentration (percolation threshold) of the second phase (NaBr in present case) until which there will be no enhancement in conductivity Once the concentration increases beyond the percolation threshold the conductivity of the system increases The experimental data obtained for NaF-NaBr system provides the direct experimental evidence for the existence of percolation threshold The percolation threshold for NaBr doped NaF mixed crystal system is between *3-5m/o*NaBr for samples cooled at the rate of 5 10°C/min Further measurements on samples prepared by controlled cooling are required to determine the percolation threshold precisely as the percolation threshold depends on the grain size[23] which obviously depends on the cooling rate

REFERENCES

1 Tubandt C and Lorentz E (1914) Z Phys Chem 87 513

2 S Chandra (1981) Superionic solids North – Holland publishing company Amsterdam

3 Kvist A (1967) Z Naturf 22a 208

4 K Shahi and J B Wagner Jr J Electrochem Soc 128 6

5 K Shahi and J B Wagner Jr (1981) Phys Rev B12 6417

6 S Chaklanobis R K Syal and K Shahi (1990) Solid State Ionics 44 107

7 G Prakash and K Shahi (1987) Solid State Ionics 23 151

8 Liang C C (1973) J Electrochem Soc 120 1289

9 K Shahi and J B Wagner Jr (1983) J Phys Chem Solids 44 89

10 Koch E and Wagner C (1937) Z Phys Chem Abt B38 295

11 Kelting H and Witt H (1949) Z Physik 126 697

12 Teltow J (1949) Ann Phys Lpz 5 63 71

13 Johanneson O and Mc Kelvy M (1985) Solid State Ionics 17 251

14 Bhima Sankaram T and Bansisir K G (1978) Crystal Lattice Defects 7 209

15 Solid State Physics A J Dekker Macmillan India press

16 1996 JCPDS – International Center for Diffraction Data

17 Physics of electrolytes, Hladik, Academic press London NewYork

18 Koch E and Wagner C (1937) Z Phys Chem B38 295

19 K Shahi and J B Wagner Jr (1983) J Solid State Chem 42 107

20 Barr L W and Lidiard A B (1970) In 'Physical Chemistry – An advanced Treatise (Ed Jost W) Academic Press New York, Vol 10 P 151

21 Maxwell J C (1881) in A Treatise on electricity and magnetism Vol 1 2nd ed Clare Don Press Oxford P 435

A133649

Date Slip

The book is to be returned on the date last stamped